Desalination and Water Treatment
www.deswater.com

doi: 10.5004/dwt.2018.21780

102 (2018) 184–196
January

Facile hydrothermally synthesized nanofibrous polyresorcinol@γ-Fe_2O_3 for dispersive ferrofluid adsorption of Cd(II): modeling and isotherm study

Mostafa Hossein Beyki, Farzaneh Shemirani*

School of Chemistry, University College of Science, University of Tehran, P.O. Box 14155-6455, Tehran, Iran, emails: shemiran@khayam.ut.ac.ir (F. Shemirani), mhosseinbaki@yahoo.com (M.H. Beyki)

Received 11 July 2017; Accepted 6 December 2017

ABSTRACT

A novel ferrofluid mediated dispersive adsorption system was developed based on a facile hydrothermally synthesized nanofibrous polyresorcinol@γ-Fe_2O_3. The nanocomposite was characterized with energy dispersive X-ray spectroscopy, X-ray diffraction, field emission scanning electron microscopy, vibrating sample magnetometer, Brunauer–Emmett–Teller and Fourier transform infrared techniques. Polysorbate and a new synthetic Schiff base were used as carrier fluid and complexing agent, respectively. To obtain effective parameters (pH, amount of sorbent and ligand and contact time) on adsorption and their interactions, response surface methodology with Box–Behnken design was used. Results confirmed that adsorption efficiency was very sensitive to pH, adsorbent dosage and amount of ligand; however, the efficiency is less sensitive to time. Under optimized conditions (pH 8; contact time 3.8 min; sorbent amount 300 μL and amount of ligand 1.3×10^{-5} mol) relative standard deviation (%) and the limit of detection was 4% and 0.13 μg L^{-1}, respectively. Reusability of the sorbent was achieved with 0.1 mol L^{-1} of HNO_3 solution. Isotherm study revealed that cadmium adsorption followed Langmuir model with maximum capacity of 56.4 mg g^{-1}. Moreover, results for Dubinin–Radushkevich and Temkin isotherm models confirmed that cadmium adsorption is a physical process. Finally developed method was used for cadmium preconcentration from water and food samples with satisfactory results.

Keywords: Cadmium; Ferrofluid; Solid phase extraction; Response surface methodology; Ultrasonic; Nanofibrous

1. Introduction

Among the various types of contaminants, heavy metals are one main category threatening aquatic lives and ecological systems as well as causing many environmental issues [1–3]. In other words, toxicity, persistency and bioaccumulation tendency of heavy metals in live tissues can pose numerous environmental and health risks by such pollutants [4,5]. Among the heavy metals, cadmium (II) is one of the most toxic metals which is released into the environment through melting and casting industries, producing metal alloys, electroplating, photography, pigment works and production of alkaline batteries [6–10]. The regular exposure of cadmium causes hypertension, liver insufficiency, bone lesions, cancer and cardiovascular diseases; hence the USA Environmental Protection Agency and the World Health Organization set a limit of 5 and 3 ppb of Cd(II) ions for drinking water [11–13]. Based on the mentioned subjects, development of reliable methods is necessary for the adsorption/determination of Cd(II) from aquatic environment. To date, various treatment techniques were developed for the removal of toxic Cd(II) including liquid–liquid extraction, adsorption, chemical precipitation, ion exchange, coagulation, reverse osmosis, electrolysis and membrane filtration [14–21]. Among the mentioned techniques, adsorption is a popular way for

* Corresponding author.

adsorption of cadmium owing to several advantages such as low cost, rapid phase separation, low consumption of organic solvents and elimination of matrix interference [22–24]. Despite the worthiness of adsorption methods, stability and efficiency of the system for adsorption of analytes as well as elimination of interfering matrix are critical [25]. For this purpose, various solid sorbents have been developed to enhance the efficiency of adsorption methods including carbon nanotube, graphene, zeolite, silica, alumina and polymeric materials [26–32]. However, adsorption with nanomaterials with high specific surface area possess very advantage but employment of them show some drawbacks including high backpressure in column dynamic extraction mode and the need to centrifuge and filter in static batch mode which made this method time consuming. To overcome such difficulties, magnetic adsorption (MA) was developed as the magnetic nanoparticles (MNPs) act as carrier of adsorbent [33,34]. In fact the superparamagnetic behavior of MNPs, allow simple and fast extraction dynamics [35,36]. In recent years, numerous researches have focused on coated MNPs with various compounds, because the coating material prevents the core part from aggregation and improves the selectivity and efficiency of MA system [37,38].

Recently, ferrofluid mediated dispersive adsorption was developed as a new technique. In fact this technique was developed based on colloidal dispersions of MNPs suspension in a carrier fluid such as water, ester ionic liquids and hydrocarbons [39–41]. Basically, in ferrofluids, the MNPs should be coated by a suitable material such as surfactants, polyelectrolytes or inorganic materials, to increase the stability of the prepared ferrofluid as well as prevent particles from agglomeration [42]. Ferrofluid stabilized with various polymers is another most employed way which use various polymer derivatives such as starch, chitosan, polyvinyl alcohol, polyethylene glycol, etc. [43].

Based on these viewpoints; polymer coated magnetic γ-Fe_2O_3 nanofibrous structure was fabricated and employed to prepare a novel adsorption system. For this purpose a one-step hydrothermal route was used for synthesis of nanofibrous magnetic polyresorcinol which stabilized with polysorbate as a novel carrier. This is a first report for employment of the synthetic nanofibrous polymer as a coating agent and polysorbate in ferrofluid mediated adsorption of cadmium from real samples. Moreover, effective parameters on cadmium adsorption, that is, pH, contact time, adsorbent dosage and amount of synthetic Schiff base as well as their interactions were studied with response surface methodology (RSM). Isotherm models were also studied and discussed in detail.

2. Experimental setup

2.1. Materials and methods

$FeCl_2.4H_2O$, $FeCl_3.6H_2O$, ammonia, resorcinol, para-formaldehyde, 2-hydroxybenzaldehyde, p-phenylenediamine, dimethylsulfoxide (DMSO) and polysorbate were purchased from Merck (Darmstadt, Germany). Ethanol was supplied from Bidestan Company (Qazvin, Iran). Standard solutions of Cd(II) ions (1,000 mg L^{-1}) were prepared by dissolving of $Cd(NO_3)_2$ salt in distilled water. NH_3 and HNO_3 solutions (0.1 mol L^{-1}) were used for adjustment of working pH. Preparation of ferrofluid was assisted with an ultrasound clean bath operating at 40 Hz with a power of 340 W (Elmasonic, type S, Singen, Germany). Flame atomic absorption spectrometer (FAA-400, Varian, Musgrave, Australia) equipped with a deuterium lamp background and hollow cathode lamp was used for the determination of cadmium ions. A digital pH meter (model 692, Metrohm, Herisau, Switzerland) was used for pH adjustment. The prepared nanomaterials were characterized by powder X-ray diffraction (XRD, X'Pert MPD, Philips, Almelo, The Netherlands) with Cu-Ka (λ = 1.540589 Å) radiation in the 2θ range of 2°–100°. Fourier transform infrared (FT-IR, Equinox 55, Bruker, Germany) spectra were measured with attenuated total reflectance at the wavelength of 400–4,000 cm^{-1}. Surface morphology analysis of the composite was carried out by field emission scanning electron microscopy (FESEM, EM10C, Zeiss, Germany). Magnetic characteristic was determined with a vibrating sample magnetometer (VSM) (Model 7400, Lake Shore, Japan). The N_2 adsorption–desorption isotherms were recorded on a Nova Station A system.

2.2. Synthesis of Schiff base and magnetic polymer

To prepare Schiff base, 2-hydroxybenzaldehyde and p-phenylenediamine with 2:1 mol ratio was dissolved in 50 mL ethanol and refluxed for 6 h along with magnetic stirring. Obtained orange precipitate was collected with filtration and washed three times with ethanol and dried at 60°C for 6 h.

A one-step hydrothermal route has been employed to prepare γ-Fe_2O_3@polyresorcinol. For this purpose, 1.0 g of resorcinol was dissolved in 50 mL of distilled water containing 3 mL of concentrated NH_3 (25% W/W). Thereinafter, 2.33 g of $FeCl_3.6H_2O$ and 0.9 g of $FeCl_2.4H_2O$ in 10 mL of distilled water has been added to the above solution and stirred for 5 min. In subsequent step, 0.5 g of p-formaldehyde has been added to the mixture and after stirring for 30 min, the reactants were transferred into a Teflon lined autoclave and heated at 180°C for 24 h. At the end of reaction, the suspension was filtered and washed with distilled water three times and with ethanol twice. The resulted gray products were dried at 70°C for 6 h. Synthetic protocol is schematically illustrated in Fig. 1.

2.3. Cadmium adsorption procedure

To prepare ferrofluid, 13 mg of magnetic polymer was added in 100 µL of acetic acid and stirred for 10 min then 0.5 mL of polysorbate was added to the suspension and

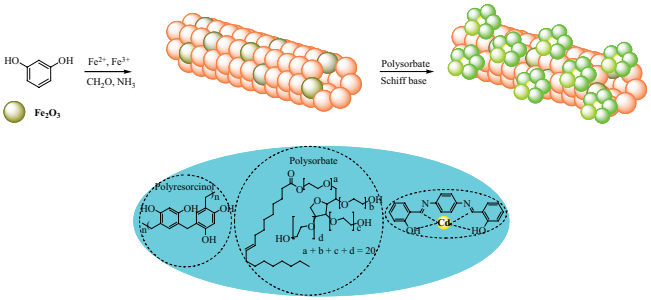

Fig. 1. Schematic illustration of magnetic composite preparation.

sonicated for about 60 min at 80°C. To optimize effective parameters on cadmium adsorption, RSM tests were performed by 29 designed run at one block. Cadmium sample volume and concentration were 20 mL and 1.0 mg L^{-1}, respectively. Four studied effective parameters include pH, contact time, adsorbent amount and mol of ligand. Design Expert software 7.0 with Box–Behnken design (BBD) was used to evaluate the effective parameters. Cadmium ions adsorption experiments have been performed with batch method. For instance, the pH of 20 mL of cadmium solution with an initial concentration of 0.01–70 mg L^{-1} was adjusted to 8, and 13 μL of Schiff base solution (10^{-3} mol L^{-1} in DMSO) was added to it. Then 300 μL ferrofluid was injected to the cadmium solution with a microsyringe and the mixture was shaked for 3.8 min. After equilibrium the sorbent was separated by external magnetic field and the concentration of cadmium ions in the supernatant or in 5 mL of HNO_3 solution as eluent (0.1 mol L^{-1}) was determined by flame atomic absorption spectroscopy (FAAS). The same procedure was applied to the blank solution. Removal percentage (%R) was calculated as follows:

$$R\% = [(C_0 - C_e) \times 100]/C_0 \quad (1)$$

where C_0 (mg L^{-1}) and C_e (mg L^{-1}) express initial concentration and remained cadmium in the solution after equilibrium, respectively.

3. Results and discussions

3.1. Characterization

The XRD analysis (Fig. 2(a)) was used to verify the crystallinity of the magnetic nanocomposite. The characteristic peaks due to Fe_2O_3 show scattering at 2θ = 30.26°, 35.34°, 43.22°, 53.55°, 57.23° and 63.32° corresponding to the (220), (311), (400), (422), (511) and (440) planes of Fe_2O_3 crystal that match well with the standard spectra (00-003-0863.CAF) [44]. The XRD was dominant with the main peaks of nanoparticles which confirmed that the coating of nanoparticles with the polymer resulted in a low effect on its crystallization. The pattern showed a main broad scattering with a maximum height at 20° which confirmed the preparation of polymer. Observed reflections could be indexed in a pseudo-orthorhombic cell [45] that ascribed to periodicity parallel to the polymer chain [46].

In the FT-IR spectrum of nanocomposite (Fig. 2(b)), peaks at 3,455 and 2,930 cm^{-1} are attributed to the stretching of –OH and –CH groups. The peaks observed at 600 cm^{-1} and 1,000–1,600 cm^{-1} are owing to the vibration of Fe–O and C=C. The spectrum of the synthetic ligand appeared to have absorbance owing to the stretching vibration of free and hydrogen bonded O–H at 3,000–3,500 cm^{-1}. Moreover, the C–H stretching, the C–O stretching and the OH bending vibration of phenolic groups could be observed at 2,923, 1,039 and 1,374 cm^{-1}, respectively. The absorption peaks at 1,441 and 1,680 cm^{-1} relate to the CH_2 symmetric scissoring and C=N vibration,

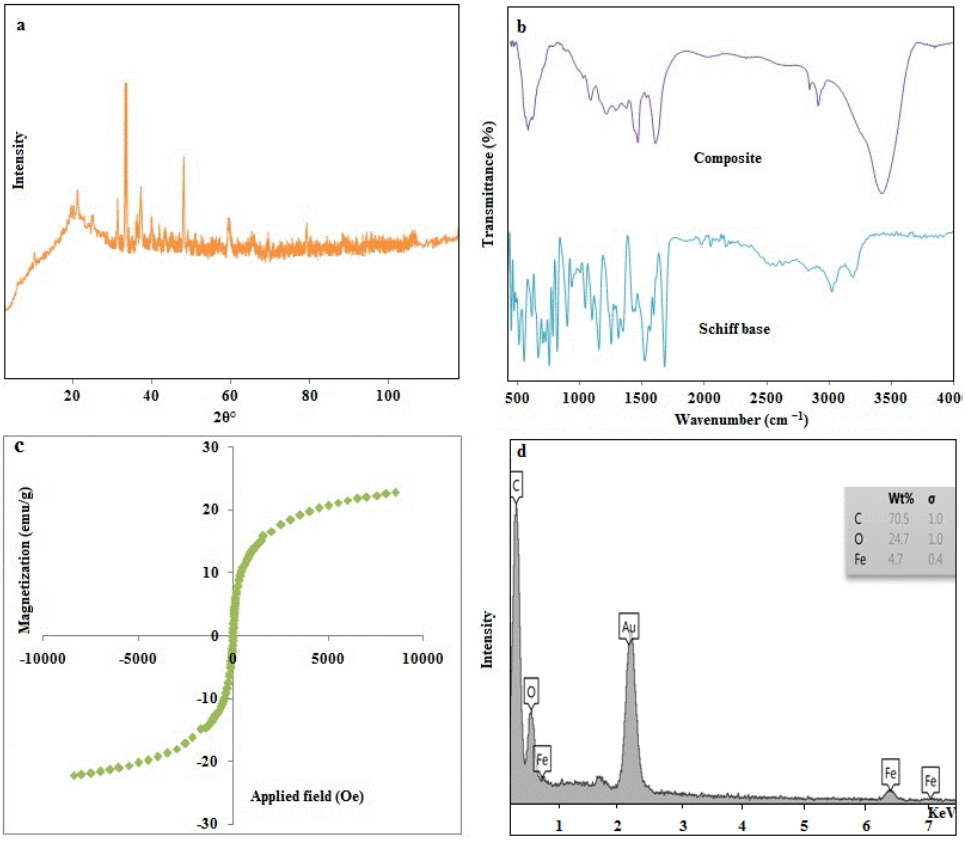

Fig. 2. XRD pattern (a), FT-IR spectra (b), VSM graph (c) and EDX spectra (d) of prepared magnetite polyresorcinol.

respectively. The C=C stretching vibrations of aromatic ring was observed at 1,400–1,600 cm^{-1}.

The magnetic hysteresis loops based on the magnetization (M) vs. the applied magnetic field (H) are shown in Fig. 2(c), as the magnetization of the materials has exhibited a clear hysteresis behavior. The magnetic nanocomposite including saturation magnetization (M_s) and remnant magnetization (M_r) could be determined from the hysteresis loops. The values of M_s for as synthesized composite is 24 emu g^{-1} which is lower than that of some reports (40 emu g^{-1}) [47]. Suppresses in saturation magnetization has been owing to disorder in magnetic moment orientation, which has resulted in dispersion in the exchange constant [48]. According to the relation between the volume fraction of the particles (Ø) and the saturation moment of a single particle (m_S), the M_s (M_s = Ø m_S) [49] is dependent on the volume fraction of the MNPs, and the contribution of the coating layers on the total magnetization. Hence presence of polymeric layer on the nanoparticle surface is a main reason of low value of M_s. It has been observed that the M_r of nanocomposite is 0.27 emu g^{-1} which has indicated that the particles probably possess superparamagnetic properties in that the remanence of the particles has been near to zero in the absence of an external magnetic field [50]. The reason for this situation is that the particle size is so small to such an extent that each particle acts as a single magnetic domain.

The results of energy dispersive X-ray spectroscopy (EDX) elemental analysis of the nanocomposite is illustrated in Fig. 2(d). As can be seen, the spectra of nanocomposite showed presence of iron, oxygen and carbon as the main component of the hybrid. The appearance of the Au in the EDX spectra (2 KeV) is from the gold supporting the nanoparticles for the FESEM recording. FESEM image of nanocomposite is shown in Fig. 3 and confirmed irregular aggregated fibers with mean diameter of 50 nm. Few amounts of semispherical components are also observable which is corresponding to MNPs in polymer structure. The structures of composite contain hydroxyl groups as well as aromatic ring, which interact with each other, thus the nanocomposite can be regarded as a combined structure [51].

The N_2 adsorption–desorption isotherm is shown in Fig. 4. As can be seen, the curve shows type II isotherm with a minor hysteresis loop as a result of filling and emptying of the mesopores by capillary condensation [52]. The Brunauer–Emmett–Teller surface area and total pore volume of composite was 153 m^2/g and 0.20 cm^3/g. Moreover, the average pore diameter of 7.0 nm confirmed that the material is classified as mesoporous compound [53]. The porosity of the prepared structure may be due to of the formation of mesoporous voids formed by the hypercrosslinking between monomers as well as aggregation of Fe_2O_3 nanoparticles due to magnetic–magnetic dipole interactions.

3.2. Optimizing effective parameter on cadmium adsorption

Effective parameters on cadmium adsorption were optimized with RSM using BBD. To run adsorption experiments Design Expert software version 7.0.0 was used. The design consists of removal percentage (%R) as response and four factors (pH: A, contact time: B, adsorbent amount: C and mol of ligand: D) as effective parameters. Prediction of response and variables interactions was described with a polynomial equation:

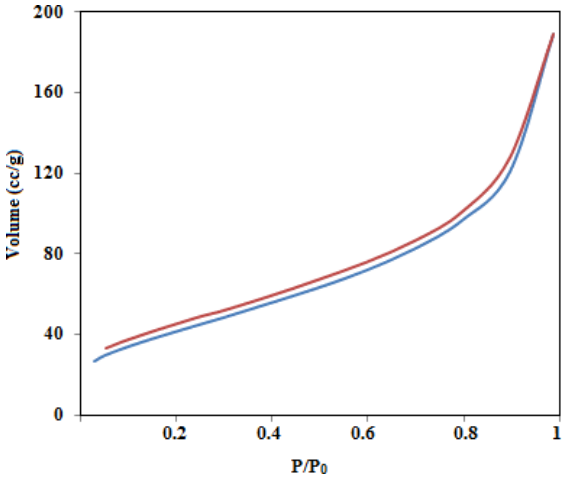

Fig. 4. N_2 adsorption–desorption isotherm of composite.

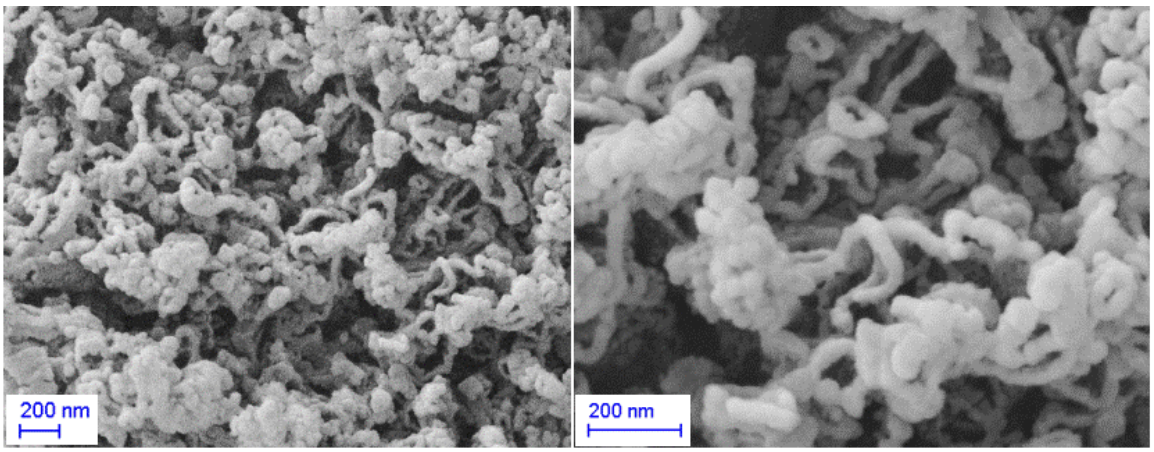

Fig. 3. FESEM image of fibrous γ-Fe_2O_3 – polyresorcinol composite.

$$Y = \beta_0 + \sum_{i=1}^{k}\beta_i X_i + \sum_{i=1}^{k}\beta_{ii} X_i^{\,2} + \sum_{i=1}^{k-1}\sum_{j=2}^{k}\beta_{ij} X_i X_{ij} \quad (2)$$

where Y is the predicted response; X_i and X_j represent the coded values of independent variables and β is the regression coefficient constant of the developed model [54]. The experimental design consisted of total 29 runs, one block and five center points. The equations were validated by the analysis of variance (ANOVA) as well as 3D response surface plots drawn for the experimental data to provide an overview of the variables effects and optimum level of parameters. The empirical relationship between removal percentage (*R*%) and the variables are as follows:

$$\begin{aligned}\%R = {} & +90.00 + 42.93A + 7.25B - 12.61C + 22.62D \\ & - 18.10AB - 0.62AC + 1.67AD + 1.38BC \\ & - 4.00BD + 17.12CD - 28.01A^2 + 2.95B^2 \\ & - 14.24C^2 - 9.58D^2 + 13.10A^2B + 18.24A^2C \\ & - 21.54A^2D - 15.82AB^2 - 2.05AC^2 + 21.74B^2C \\ & - 20.61B^2D - 0.88BC^2\end{aligned} \quad (3)$$

According to the results of ANOVA calculation in Table 1, the regressions for the adsorption of cadmium were statistically significant since the F value is 63.55 with a low probability value ($P < 0.0001$). Based on *p* values of each model term, the independent variables, that is, pH, contact time, amount of adsorbent and ligand significantly affected the adsorption efficiency. The plot of predicted response against observed values in Fig. 5(a) showed a good agreement of the response (%*R*) over the selected range of independent variables. Most of the response points are located in narrow range as the value of standard deviation between the experimental and predicted results is 4.72. Moreover, there is a good agreement between R^2 (0.99) and adjusted R^2 (0.98) value which indicated a high dependence and correlation between the observed and the predicted response [55]. The signal to noise ratio or adequate precision is 23.48 that confirmed the significance of model since the ratio greater than 4 is desirable. Normal probability plot was used to check the validity of ANOVA [56]. Results in Fig. 5(b) showed a straight line and low violation of the assumptions underlying the analysis, and confirms the normality of the data. Perturbation plots at Fig. 5(c) show a steep curvature in pH, amount of adsorbent and ligand which confirmed that the response was very

Table 1
Analysis of variance (ANOVA) for the Box–Behnken design

Source	Sum of Squares	df	Mean square	F value	*P* value Probability > F	
Model	31,145.62	22	1,415.71	63.55	<0.0001	Significant
A-pH	7,370.22	1	7,370.22	330.84	<0.0001	
B-Time	210.25	1	210.25	9.44	0.0219	
C-Dosage	636.55	1	636.55	28.57	0.0018	
D-Ligand	2,045.75	1	2,045.75	91.83	<0.0001	
AB	1,310.44	1	1,310.44	58.82	0.0003	
AC	1.56	1	1.56	0.070	0.8000	
AD	11.22	1	11.22	0.50	0.5045	
BC	7.56	1	7.56	0.34	0.5814	
BD	64.00	1	64.00	2.87	0.1410	
CD	1,171.69	1	1,171.69	52.60	0.0003	
A^2	5,089.04	1	5,089.04	228.44	<0.0001	
B^2	56.54	1	56.54	2.54	0.1622	
C^2	1,315.78	1	1,315.78	59.06	0.0003	
D^2	595.31	1	595.31	26.72	0.0021	
A^2B	343.22	1	343.22	15.41	0.0078	
A^2C	665.40	1	665.40	29.87	0.0016	
A^2D	927.94	1	927.94	41.65	0.0007	
AB^2	500.86	1	500.86	22.48	0.0032	
AC^2	8.40	1	8.40	0.38	0.5616	
B^2C	945.26	1	945.26	42.43	0.0006	
B^2D	849.96	1	849.96	38.15	0.0008	
BC^2	1.53	1	1.53	0.069	0.8020	
Residual	133.66	6	22.28			
Lack of fit	7.17	2	3.58	0.11	0.8957	Not significant
Pure error	126.50	4	31.63			
Cor total	31,279.28	28				

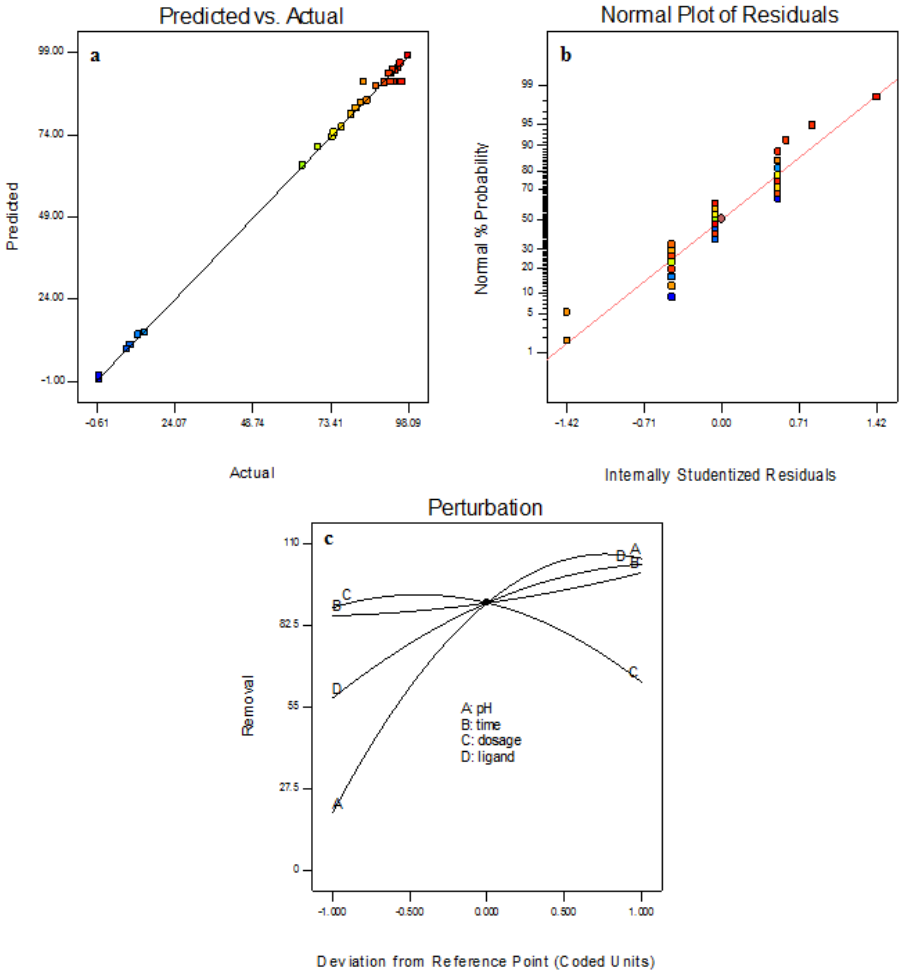

Fig. 5. The plot of prediction response value vs. actual (a), normal probability plot (b) and perturbation plot (c) of cadmium adsorption with the ferrofluid mediated system.

sensitive to these factors. The small curvature of the time plot shows slight sensitivity of the responses to the change in this variable.

Effect of variable parameters on adsorption efficiency was further studied with three-dimensional response surfaces in Fig. 6. According to the results (from the 3D plots of pH–time, pH–dosage and pH–mol of ligand in Figs. 6(a)–(c)), it can be seen that the solution pH is a very effective parameter since in the pH range from 3 to 8, mean removal efficiency was in the range of 0.1%–96%. Observed results can be explained with the fact that at acidic solution the hydroxyl functional groups on the sorbent surface as well as C=N and OH groups on the Schiff base structure is fully protonated. In other words, high concentration of H^+ is a competitive factor which prevents cadmium adsorption on the surface of the sorbent. With increase of pH, the OH groups may be in deprotonated form which can easily interact with cadmium ions through complexation. At the subsequent step cadmium–Schiff base complex species can be adsorbed on the sorbent surface through hydrophobic and π–π interactions between bulk π systems on phenolic ring and ligand molecule. Hydrogen bonds because of the functional groups on the polymer surfaces also participate in cadmium–Schiff base complex adsorption. In other words, for polyresorcinol as a polar organic compound, the Schiff base adsorption tends to increase with increased potential H bonding sites (–N, –OH) on the reactant structure [57].

Contact time was designed in the range of 1–15 min with central point of 8 min. From the results (the 3D plots of pH–time, time–adsorbent amount and time–mol of ligand in Figs. 6(a), (d) and (e)), it can be seen that with increasing shacking time removal percentage was increased. Moreover, it can be seen that initial uptake is also high that could be attributed to the external surface adsorption of cadmium–Schiff base complex, and absence of internal diffusion resistance [58]. The fast extraction rate indicates that the system is highly suitable for the preconcentration of cadmium from aqueous solutions.

The amount of adsorbent was also designed in the range of 5–20 mg. It is observed that (from the 3D plot of pH–adsorbent amount, time–adsorbent amount, adsorbent amount–mol of ligand in Figs. 6(b), (d) and (f)) the removal efficiencies increased as the amount of sorbents increased and then reached a steady state. Increase in adsorption efficiency with adsorbent dosage is owing to the availability of higher binding sites on the sorbent surface.

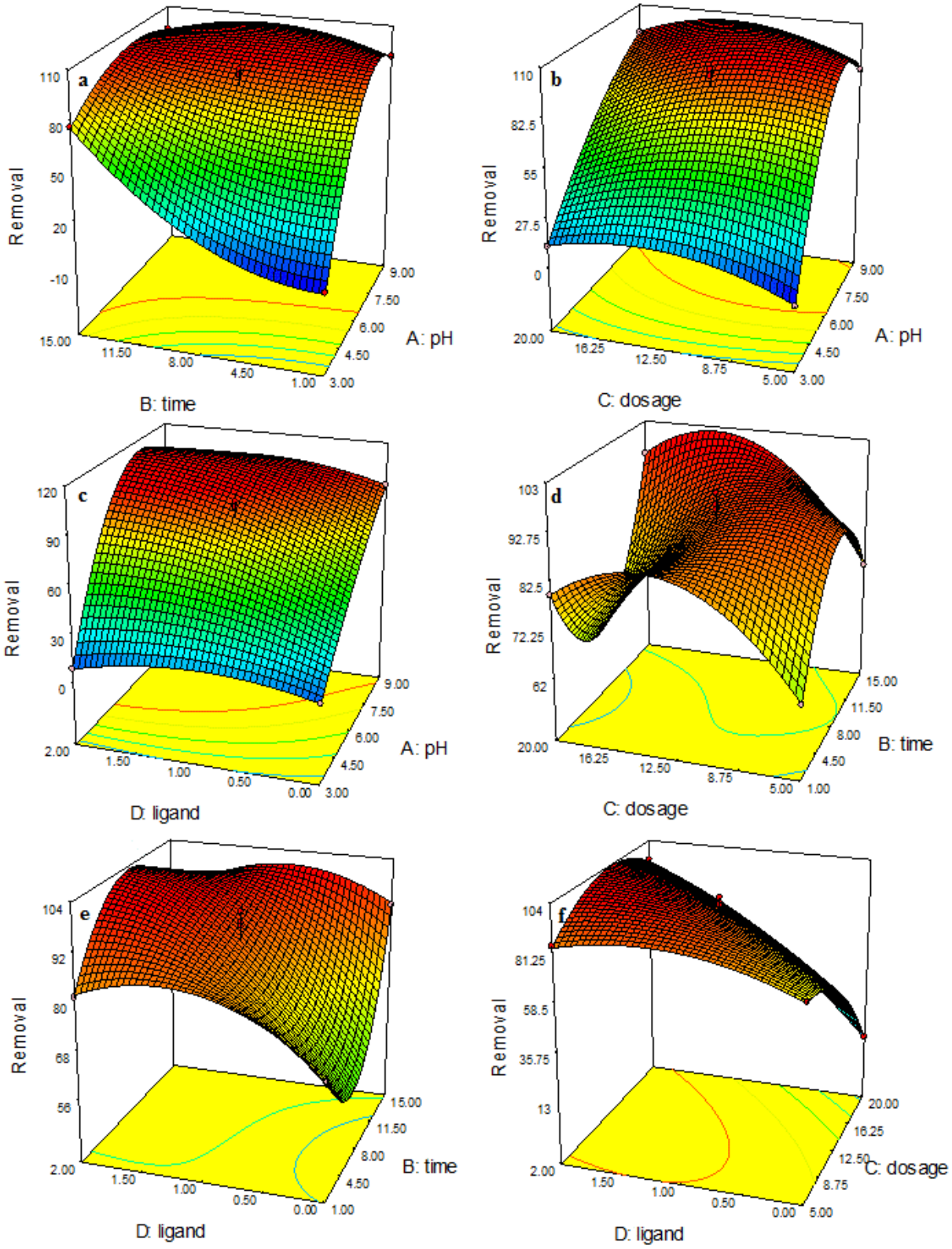

Fig. 6. 3D plot for pH and time while adsorbent amount and mol of ligand were fixed at optimum values (a), 3D plot for pH and adsorbent amount while time and mol of ligand were fixed at optimum values (b), 3D plot for pH and mol of ligand while time and adsorbent amount were fixed at optimum values (c), 3D plot for time and adsorbent amount while pH and mol of ligand were fixed at optimum values (d), 3D plot for time and mol of ligand while pH and adsorbent amount were fixed at optimum values (e), 3D plot for adsorbent amount and mol of ligand while pH and time were fixed at optimum values (f).

The amount of ligand was fixed in the range of 0–2 × 10^{-5} mol. As shown in Figs. 6(c), (e) and (f), adsorption of cadmium increased upon addition of ligand. This owes to increase of complexation probability with the increase of ligand concentration.

To evaluate the accuracy of the results obtained by the model, under optimum condition (pH, 8; contact time, 3.8 min; sorbent amount, 300 μL and amount of ligand, 1.3 × 10^{-5} mol), three experiments were carried out and results showed a good agreement between the optimum-calculated response (102%) and mean experimental response (96%).

To evaluate the role of ligand on cadmium adsorption, the experiment at initial concentration of 1 mg L^{-1} in absence and presence of ligand was performed. Result showed that removal efficiency was 88% in absence of ligand which reached to 99% in the presence of ligand at optimum level (1.3 × 10^{-5} mol). This may be assigned to the multiple adsorption sites which are ready to capture cadmium ions. In other words, the nanocomposite contains hydroxy and amine groups which act as electron donor fragment which interact with cadmium ions as electron acceptor species. Besides synthetic Schiff base also assists cadmium adsorption with higher efficiency than naked composite which confirmed synergism of both fragments to enhance cadmium adsorption efficiency.

3.3. Isotherm study and error analysis

The effect of cadmium concentration on the sorption was analyzed in the concentration between 0.1 and 70 mg L^{-1}. Results in Fig. 7(a) showed that with increase in initial cadmium concentration adsorption percentage decreases as the efficiency reached from 100% at initial concentration of 0.1 mg L^{-1} to 35% at initial concentration of 70 mg L^{-1}. Cadmium adsorption was further analyzed in terms of Langmuir and Freundlich models [59–61]. Langmuir and Freundlich isotherm models are illustrated as follows:

$$Q_e = bQ_m C_e/(1 + bC_e) \quad (4)$$

$$Q_e = K_f C_e^{1/n} \quad (5)$$

In these equations, C_e is the amount of analyte in the liquid phase at equilibrium (mg L^{-1}) and Q_e is the amount of analyte adsorbed per unit mass of the sorbent (mg g^{-1}). Q_m is the maximum adsorption capacity, b is the Langmuir coefficient as well as n and K_f are the Freundlich coefficients [62–64]. Results of the linear adsorption isotherm models of Langmuir and Freundlich at optimum conditions (pH of 8,

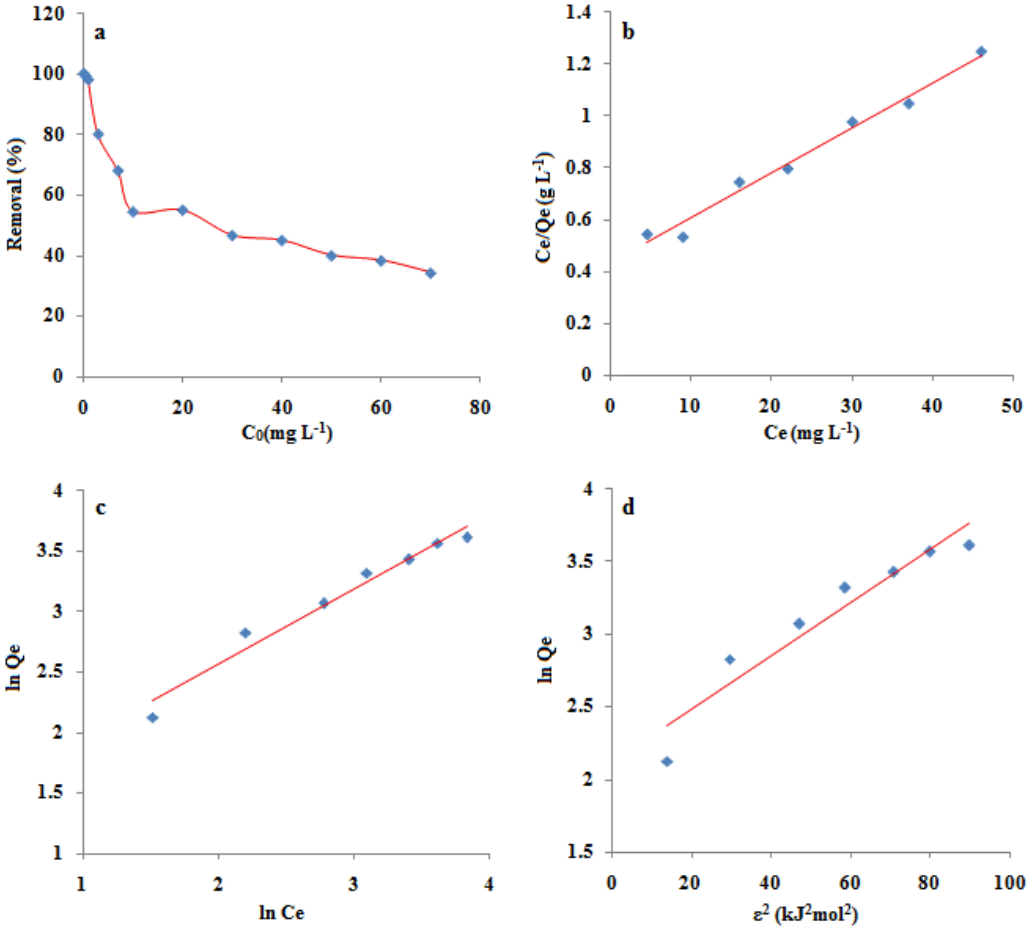

Fig. 7. Effect of cadmium concentration on adsorption efficiency (a), linear Langmuir isotherm (b), linear Freundlich isotherm model (c) and D–R isotherm model (d) for cadmium adsorption.

shacking time of 3.8 min, adsorbent amount of 300 μL and amount of ligand: 1.3×10^{-5} mol) are presented in Figs. 7(b) and (c). As can be seen, the adsorption followed Langmuir model with R^2 value of 0.982. However the Freundlich model also has high linearity hence statistic error analysis was employed to select best adsorption model to describe cadmium adsorption onto magnetic polymer surface. For this purpose, sum of squared errors (SSE) equation was employed.

$$SSE = \Sigma(Q_{exp} - Q_c)^2 \quad (6)$$

In this equation, Q_{exp} and Q_c are the experimental adsorption capacity data, and are calculated from nonlinear model. According to results at Table 2, the SSE value for Langmuir and Freundlich models is 5.8 and 15.21, respectively. These results confirmed that cadmium adsorption followed monolayer adsorption onto homogeneous surface. Essential characteristics of the Langmuir equation could be expressed by equilibrium parameter, R_L, which is a dimensionless constant.

$$R_L = 1/(1 + K_L C_0) \quad (7)$$

Table 2
Isotherm models and their parameter values

Models	Parameters	Values
Langmuir	R^2	0.991
	Q_m	56.47
	B	0.042
	R_L	0.25–0.70
	SSE	5.80
Freundlich	R^2	0.976
	N	1.83
	K_f	4.79
	SSE	15.21
D–R	R^2	0.915
	Q_m	56.45
	E	5.29
Temkin	R^2	0.989
	B	12.48
	A_T	0.414
Redlich–Peterson	R^2	0.991
	K_R	2.41
	A	0.045
	B	0.98
Sips	R^2	0.991
	K_s	2.88
	Q_m	56.47
	n	68.4
Hill	R^2	0.991
	Q_{sH}	56.4
	K_D	23.76
	n_H	1.001

In this equation, C_0 is the initial solute concentration. The value of R_L indicates the isotherm to be irreversible ($R_L = 0$), favorable ($0 < R_L < 1$), linear ($R_L = 1$) or unfavorable ($R_L > 1$) [65]. Result confirmed that cadmium adsorption onto sorbent is favorable.

The Dubinin–Radushkevich (D–R) isotherm model which has been used to distinguish physical from chemical adsorption is given by the following equations:

$$\ln Q_e = \ln Q_{max} - \beta\varepsilon^2 \quad (8)$$

$$E = -1/(-2\beta)^{1/2} \quad (9)$$

$$\varepsilon = RT\ln(1 + 1/C_e) \quad (10)$$

where β stands for the activity coefficient related to mean adsorption energy ($mol^2\ kJ^2$) and ε is the Polanyi potential ($kJ^2\ mol^2$). R and T are the gas constant (8.314 J $mol^{-1}\ K^{-1}$) and the absolute temperature (K) [66]. Results are depicted in Fig. 7(d) and Table 2 and can be seen that the value of mean free energy is 5.29 kJ mol^{-1} which lies in the range of 1–8 kJ mol^{-1} indicates that the adsorption of Cd^{2+} followed a physical type.

Temkin isotherm contains a factor that explicitly takes into account the adsorbent–adsorbate interactions. The model assumes that heat of adsorption of all molecules in the layer would decrease linearly rather than logarithmic with coverage. The model is given by the following equation:

$$Q_e = B\ln A_T + B\ln C_e \quad (11)$$

where A_T and B are Temkin isotherm equilibrium binding constant (L g^{-1}) and constant related to heat of sorption (J mol^{-1}), respectively [67].

According to the results, the values of A and B are 0.414 and 12.48 which shows that cadmium adsorption is a physical process.

The Redlich–Peterson is a three-parameter isotherm which combines both Langmuir and Freundlich isotherms. The equation is given as:

$$Q_e = K_R C_e/(1 + \alpha_R C_e^{\beta}) \quad (12)$$

where K_R (L/g) and α_R (L/mg) are Redlich–Peterson isotherm constants and β is the exponent which lies between 0 and 1. It approaches the Freundlich model at high concentration ($\beta = 0$) and is in accord with the low concentration limit of the Langmuir equation ($\beta = 1$) [68,69]. It can be seen that the value of β is near to 1 which confirmed that cadmium adsorption followed monolayer Langmuir model.

Sips isotherm is also a combined form of Langmuir and Freundlich expressions deduced for predicting the heterogeneous adsorption systems [70]. At low adsorbate concentrations, it reduces to Freundlich isotherm; while at high concentrations, it predicts a monolayer adsorption capacity characteristic of the Langmuir isotherm.

$$Q_e = Q_{max} K_S C_e^{1/n}/1 + K_S C_e^{1/n} \quad (13)$$

where K_S is the Sips constant related with affinity constant $(mg\ L^{-1})^{-1/n}$ and Q_{max} is the Sips maximum adsorption capacity (mg g^{-1}).

Hill equation was postulated to describe the binding of different species onto homogeneous substrates.

$$Q_e = Q_{sH}C_e^{nH}/K_D + C_e^{nH} \quad (14)$$

where K_D, n_H and Q_{sH} are constants. The model assumes that adsorption is a cooperative phenomenon, with the ligand binding ability at one site on the macromolecule may influence different binding sites on the same macromolecule [71].

The theoretical data for the studied isotherm models were extracted using MATLAB R2013a software and the results are presented in Table 2. Based on its R^2 values, the theoretical data yielded excellent fits in the following isotherms order: Redlich–Peterson > Sips > Hill > Langmuir > Temkin > Freundlich > D–R. Results for isotherm study showed that presented adsorption system has large adsorption capacity for cadmium uptake which made the system an appropriate candidate for cadmium remediation.

3.4. Effect of interfering ions

There are many different anions and cations in real sample matrixes which can interact with the adsorbent or the adsorbate and consequently lead to decrease in extraction efficiency [72]. Thus, the effects of interfering ion on the extraction of analytes were investigated by adding a known quantity of the desired ions to a 20 mL aliquot of the analyte aqueous solution with concentration of 0.1 mg L^{-1}. The tolerance limit of coexisting ions is defined as the largest amount that makes the recovery of the analyte less than 90%. The results in Table 3 indicate that the tested ions were not found to interfere with the extraction process in the range of their amounts tested. These results proved the applicability of the proposed method for determination of cadmium ion in complicated matrix samples.

3.5. Regeneration and figure of merits

In order to release cadmium ions from sorbent surface, different concentration of HCl and HNO_3, that is, 0.1 and 0.2 mol L^{-1} were used. It was found that 0.1 mol L^{-1} of HNO_3 can easily desorb cadmium ions as a result it was employed as eluent in subsequent experiments. To evaluate reusability of the sorbent, adsorption/desorption was performed under the selected optimum conditions by shacking the optimum value of the sorbent in 5 mL of HNO_3 (0.1 mol L^{-1}) as eluent. The results showed that the nanohybrid is stable and reusable up to four times (>90%) without any significant loss in the recovery of the studied metal ion. In order to evaluate the stability of magnetic iron composite after elution experiment, the adsorbent was separated and amount of dissolved iron ions in the supernatant solution was determined by FAAS. It was found that after three cycles only 3.5%–4% iron was dissolved which shows good stability for magnetic composite. Moreover, FESEM image of composite is provided in Fig. 8. It can be seen that morphology of nanocomposite did not significantly change after regeneration experiment which confirmed it had good stability.

To obtain calibration curve, different initial concentration of cadmium was constructed according to adsorption experiment and it was found that linearity in the final solution was at 0.5–100 μg L^{-1}. The coefficient of determination (R^2) was 0.991 for Cd(II). The limit of detection (LOD) was defined as LOD = $3S_B/m$ where S_B is the standard deviation of six replicates blank signals, and m is the slope of the calibration curve after preconcentration [73]. The limit of detection was found to be 0.13 μg L^{-1} and relative standard deviation (%RSD) was 4%.

3.6. Application to real samples

The accuracy and precision of developed procedure was evaluated by determination of cadmium ions in well water, liver and lettuce. Amounts of 0.2 g of liver and 5.0 g of lettuce were dissolved in 10 mL of 65% nitric acid by heating at 70°C for 45 min. After that 10 mL of 30% hydrogen peroxide was added to the solutions and the digestion flask was heated slightly until the sample solutions became clears. After cooling and filtration they were made up to volume in a 100 mL flask and 50 mL of the samples were analyzed according to general procedure. Accuracy of the method was evaluated by spiking 100 μg L^{-1} of Cd(II) in 50 mL of the sample volume. Results are depicted in Table 4. The recovery of spiked

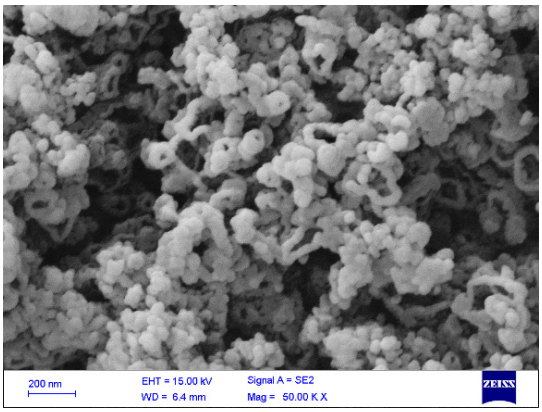

Fig. 8. FESEM image of composite after desorption experiment.

Table 3
Effect of the interfering ions on Cd^{2+} preconcentration (sorbent amount = 13 mg, time = 3.8 min, Cd^{2+} concentration = 100 μg L^{-1}, pH = 8, volume = 50 mL)

Ion	Ratio ion/Cd
Na^+, K^+	2,600
Ca^{2+}, Mg^{2+}	900
Cr^{3+}, Ni^{2+}, Co^{2+}, Cu^{2+}	20
PO_4^{3-}, NO_3^-	2,600, 1,500

Table 4
Analytical results for determination of cadmium ions in real samples after preconcentration (sorbent = 13 mg, time = 3.8 min, pH = 8, volume = 50 mL)

Sample	Added (μg L^{-1})	Found (μg L^{-1})	Recovery (%)
Well	0	–	–
water	100	97	97 ± 1
Liver	–	6	–
	100	94	88 ± 1
Lettuce	–	5	–
	100	97	92 ± 1

Table 5
Comparison the cadmium adsorption property of prepared composite with some sorbents

Adsorbent	RSD (%)	LOD μg L^{-1}	Time (min)	Linear range (μg L^{-1})	Reference
Activated carbon bovine serum albumin	3.8	0.25	24h	0.84–275	[9]
Liquid–Liquid microextraction	4.2	0.69	10	-	[15]
Poly(2-amino thiophenol)/MWCNTs	2.4	0.3	6	1–100	[32]
Modified cobalt nanoparticles	2.2	0.6	5	1–500	[38]
Fe_3O_4 – TiO_2 – PAN	2.4	0.21	8	1–110	[41]
Magnetic fibrous polymer	4.0	0.13	3.8	0.5–100	This work

samples is satisfactory (in the range of 88%–97%), which indicates the capability of the system to determine cadmium ions in real samples with different matrices.

3.7. Comparison with other methods

In Table 5, the performances of the presented method for cadmium preconcentration were compared with some reports in the literature. Results showed that the performance of the method is in good level especially respected to the equilibrium time and LOD. These results confirmed the potential of the method for cadmium determination from real samples.

4. Conclusions

In this research nanofibrous magnetite polyresorcinol was synthesized by one-step hydrothermal reaction and was demonstrated as a novel system for cadmium adsorption and preconcentration based on ferrofluid mediated magnetic solid-phase extraction. Polysorbate was used as a new carrier and synthetic Schiff base as complexation agent. RSM was employed to investigate effective adsorption parameters and their interaction. Result showed that solution pH, adsorbent amount, mol of ligand and time are main factors which affects cadmium adsorption behavior. Adsorption of cadmium is fast as equilibrium reached within 3.8 min. Seven isotherm models were studied and results showed that based on the R^2 values the experimental data fits in the following isotherms order: Redlich–Peterson > Sips > Hill > Langmuir > Temkin > Freundlich > D–R. Moreover, maximum adsorption capacity of 56.4 mg g^{-1} was obtained for cadmium uptake onto nanocomposite. Regeneration study showed the sorbent is reusable for four times of sorption and desorption with recovery more than 90%. Moreover the presented solid-phase extraction system showed good efficiency for cadmium preconcentration from real samples.

Acknowledgments

The authors would like to acknowledge the Iran National Science Foundation (INSF) (Project 94009890) as well as Research Council of the University of Tehran for the financial support of this work.

References

[1] C. Tan, Z. Zeyu, H. Rong, M. Ruihong, W. Hongtao, L. Wenjing, Adsorption of cadmium by biochar derived from municipal sewage sludge: impact factors and adsorption mechanism, Chemosphere, 134 (2015) 286–293.
[2] S.S. Rath, S. Singh, D.S. Rao, B.B. Nayak, B.K. Mishra, Adsorption of heavy metals on a complex Al-Si-O bearing mineral system: insights from theory and experiments, Sep. Purif. Technol., 186 (2017) 28–38.
[3] H.S. Ibrahim, N.S. Ammar, M. Soylak, M. Ibrahim, Removal of Cd(II) and Pb(II) from aqueous solution using dried water hyacinth as a biosorbent, Spectrochim. Acta, Part A, 96 (2012) 413–420.
[4] I. Hotan, S. Mohammad, M. Kumar, M. Ali, Z. Abdullah, M. Abulhassan, Synthesis, characterization of PMDA/TMSPEDA hybrid nano-composite and its applications as an adsorbent for the removal of bivalent heavy metals ions, Chem. Eng. J., 270 (2015) 9–21.
[5] H.A. Shaheen, H.M. Marwani, E.M. Soliman, Selective solid phase extraction and determination of trace Pd(II) using multi-walled carbon nanotubes modified with 8-aminoquinoline, J. Mol. Liq., 232 (2017) 139–146.
[6] Z. Bujn, P. Baláz, A. Zorkovská, Z. Danková, J. Brianc, Adsorption of cadmium (II) on waste biomaterial, J. Colloid Interface Sci., 454 (2015) 121–133.
[7] A. Ebrahimi, M. Ehteshami, B. Dahrazma, Isotherm and kinetic studies for the biosorption of cadmium from aqueous solution by *Alhaji maurorum* seed, Proc. Saf. Environ. Protect., 98 (2015) 374–382.
[8] G. Zeng, Y. Liu, L. Tang, G. Yang, Y. Pang, Y. Zhang, Y. Zhou, Enhancement of Cd (II) adsorption by polyacrylic acid modified magnetic mesoporous carbon, Chem. Eng. J., 259 (2015) 153–160.
[9] F. Shah, N. Ullah, T.G. Kazi, R.A. Khan, M. Sayed, H.I. Afridi, K.H. Shah, J. Nisar, Preconcentration of cadmium and manganese in biological samples based on a novel restricted access sorbents, J. Ind. Eng. Chem., 48 (2016) 180–185.
[10] J. Huang, Z. Wu, L. Chen, Y. Sun, Surface complexation modeling of adsorption of Cd(II) on graphene oxides, J. Mol. Liq., 209 (2015) 753–758.
[11] T.A. Khan, S.A. Chaudhry, I. Ali, Equilibrium uptake, isotherm and kinetic studies of Cd(II) adsorption onto iron oxide activated red mud from aqueous solution, J. Mol. Liq., 202 (2015) 165–175.
[12] S. Wu, K. Zhang, X. Wang, Y. Jia, B. Sun, T. Luo, F. Meng, Z. Jin, D. Lin, W. Shen, L. Kong, J. Liu, Enhanced adsorption of cadmium ions by 3D sulfonated reduced graphene oxide, Chem. Eng. J., 262 (2015) 1292–1302.
[13] F.A. Al-khaldi, B. Abusharkh, M. Khaled, M. Ali, M.S. Nasser, A. Saleh, S. Agarwal, I. Tyagi, V. Kumar, Adsorptive removal of cadmium (II) ions from liquid phase using acid modified carbon-based adsorbents, J. Mol. Liq., 204 (2015) 255–263.
[14] A. Zayed, M. Badruddoza, Z. Bin, Z. Shawon, T. Wei, J. Daniel, K. Hidajat, M. Shahab, Fe_3O_4/cyclodextrin polymer nanocomposites for selective heavy metals removal from industrial wastewater, Carbohydr. Polym., 91 (2013) 322–332.
[15] D.K. Osman Arslan, C. Karadaş, Simultaneous preconcentration of copper and cadmium by dispersive liquid–liquid microextraction using N,N'-bis (2-hydroxy-5-bromo-benzyl)1,2 diaminopropane and their determination by flame atomic absorption spectrometry, J. AOAC Int., 99 (2016) 1356–1362.
[16] Y. Xia, L. Meng, Y. Jiang, Y. Zhang, X. Dai, M. Zhao, Facile preparation of MnO_2 functionalized baker's yeast composites

and their adsorption mechanism for cadmium, Chem. Eng. J., 259 (2015) 927–935.
[17] T.S. Anirudhan, F. Shainy, Adsorption behaviour of 2-mercaptobenzamide modified itaconic acid-grafted-magnetite nanocellulose composite for cadmium (II) from aqueous solutions, J. Ind. Eng. Chem., 32 (2015) 157–166.
[18] L. Alves, F. De Souza, Application of constrained mixture design and Doehlert matrix in the optimization of dispersive liquid-liquid microextraction assisted by ultrasound for preconcentration and determination of cadmium in sediment and water samples by FAAS, Microchem. J., 130 (2017) 56–63.
[19] H. Kahe, M. Chamsaz, G.H. Rounaghi, A microextraction method based on ligandless ion-pair formation for measuring the cadmium cation in real samples by flame atomic absorption spectrometry, Food Anal. Methods, 9 (2016) 2887–2895.
[20] M.O. Ojemaye, O.O. Okoh, A.I. Okoh, Adsorption of Cu^{2+} from aqueous solution by a novel material; azomethine functionalized magnetic nanoparticles, Sep. Purif. Technol., 183 (2017) 204–215.
[21] I. Soylak, M. Narin, On-line preconcentration system for cadmium determination in environmental samples by flame atomic absorption spectrometry, Chem. Anal., 50 (2005) 705–715.
[22] S.A. Rezvani, A. Soleymanpour, Application of L-cystine modified zeolite for preconcentration and determination of ultra-trace levels of cadmium by flame atomic absorption spectrometry, J. Chromatogr. A, 1436 (2016) 34–41.
[23] H. Shirkhanloo, M. Falahnejad, H.Z. Mousavi, On-line ultrasound-assisted dispersive micro-solid-phase extraction based on amino bimodal mesoporous silica nanoparticles for the preconcentration and determination of cadmium in human biological samples, Biol. Trace Elem. Res., 171 (2016) 472–481.
[24] R. Nagarajah, K.T. Wong, G. Lee, K.H. Chu, Y. Yoon, N.C. Kim, M. Jang, Synthesis of a unique nanostructured magnesium oxide coated magnetite cluster composite and its application for the removal of selected heavy metals, Sep. Purif. Technol., 174 (2017) 290–300.
[25] V. Yilmaz, H. Yilmaz, Z. Arslan, J. Leszczynski, Novel imprinted polymer for the preconcentration of cadmium with determination by inductively coupled plasma mass spectrometry, Anal. Lett., 50 (2016) 1–36.
[26] E. Yilmaz, I. Ocsoy, N. Ozdemir, M. Soylak, Bovine serum albumin-Cu(II) hybrid nanoflowers: an effective adsorbent for solid phase extraction and slurry sampling flame atomic absorption spectrometric analysis of cadmium and lead in water, hair, food and cigarette samples, Anal. Chim. Acta, 906 (2016) 110–117.
[27] S. Sivrikaya, M. Imamoglu, S.Z. Yıldız, D. Kara, Novel functionalized silica gel for on-line preconcentration of cadmium (II), copper (II), and cobalt (II) with determination by flame atomic absorption spectrometry, Anal. Lett., 49 (2016) 943–957.
[28] A.J. Chem, A. Mirabi, D.A.S. Rad, D.M.R. Jamali, N. Danesh, Use of modified g-alumina nanoparticles for the extraction and preconcentration of trace amounts of cadmium ions, Aust. J. Chem., 69 (2016) 314–318.
[29] S.Z. Mohammadi, R. Roohparvar, M.A. Taher, Simultaneous separation preconcentration and determination of trace amounts of mercury and cadmium in fruits, vegetables and biological samples, J. Anal. Chem., 71 (2016) 42–49.
[30] M. Chatterjee, B. Srivastava, M.K. Barman, B. Mandal, Combined cation-exchange and solid phase extraction for the selective separation and preconcentration of zinc, copper, cadmium, mercury and cobalt among others using azo-dye functionalized resin, J. Chromatogr. A, 1440 (2016) 1–14.
[31] E. Igberase, P. Osifo, Equilibrium, kinetic, thermodynamic and desorption studies of cadmium and lead by polyaniline grafted cross-linked chitosan beads from aqueous solution, J. Ind. Eng. Chem., 26 (2015) 340–347.
[32] M. Reza, R. Sedghi, A. Bagheri, M. Behbahani, Preparation and application of poly (2-amino thiophenol)/MWCNTs nanocomposite for adsorption and separation of cadmium and lead ions via solid phase extraction, J. Hazard. Mater., 203–204 (2012) 93–100.
[33] Y. Tu, S. Ju, P. Wang, Flame atomic absorption spectrometric determination of copper, lead, and cadmium in Gastrodiae rhizoma samples after preconcentration using magnetic solid-phase extraction, Spectrosc. Lett., 49 (2016) 249–256.
[34] M.M.A. El-latif, A.M. Ibrahim, M.S. Showman, R.R.A. Hamide, Alumina/iron oxide nano composite for cadmium ions removal from aqueous solutions, Int. J. Nonferrous Metall., 2 (2013) 47–62.
[35] Z. Panjali, A.A. Asgharinezhad, H. Ebrahimzadeh, N. Jalilian, R. Yarahmadi, S.J. Shahtaheri, A simple and fast method based on new magnetic ion imprinted polymer as a highly selective sorbent for preconcentration and determination of cadmium in environmental samples, Iran. J. Public Health, 45 (2016) 1044–1053.
[36] M.J. Pirouz, M.H. Beyki, F. Shemirani, Anhydride functionalized calcium ferrite nanoparticles: a new selective magnetic material for enrichment of lead ions from water and food samples, Food Chem., 170 (2015) 131–137.
[37] F. Ge, M. Li, H. Ye, B. Zhao, Effective removal of heavy metal ions Cd^{2+}, Zn^{2+}, Pb^{2+}, Cu^{2+} from aqueous solution by polymer-modified magnetic nanoparticles, J. Hazard. Mater., 211–212 (2012) 366–372.
[38] M. Roushani, Y.M. Baghelani, S. Abbasi, M. Mavaei, S.Z. Mohammadi, Flame atomic absorption spectrometric determination of cadmium in vegetable and water samples after preconcentration using magnetic solid-phase extraction, Int. J. Veg. Sci., 5260 (2017) 304–320.
[39] M. Davudabadi Farahani, F. Shemirani, Ferrofluid based dispersive-solid phase extraction for spectrophotometric determination of dyes, J. Colloid Interface Sci., 407 (2013) 250–254.
[40] M.D. Farahani, F. Shemirani, M. Gharehbaghi, Ferrofluid-based dispersive solid phase extraction of palladium, Talanta, 109 (2013) 121–127.
[41] N. Fasih Ramandi, F. Shemirani, Selective ionic liquid ferrofluid based dispersive-solid phase extraction for simultaneous preconcentration/separation of lead and cadmium in milk and biological samples, Talanta, 131 (2015) 404–411.
[42] M. Alvand, F. Shemirani, Fabrication of Fe_3O_4 @ graphene oxide core-shell nanospheres for ferrofluid-based dispersive solid phase extraction as exemplified for Cd (II) as a model analyte, Microchim. Acta, 183 (2016) 1749–1757.
[43] S. García-jimeno, J. Estelrich, Ferrofluid based on polyethylene glycol-coated iron oxide nanoparticles: characterization and properties, Colloids Surf. A, 420 (2013) 74–81.
[44] M. Shirkhodaie, M. Hossein Beyki, F. Shemirani, Biogenic synthesis of magnetic perlite@iron oxide composite: application as a green support for dye removal, Desal. Wat. Treat., 57 (2016) 11859–11871.
[45] J.P. Pouget, M.E. Jozefowicz, A.J. Epstein, X. Tang, S.G. MacDiarmid, X-ray structure of polyaniline, Macromolecules, 24 (1991) 779–789.
[46] Q.H. Zeng, D.Z. Wang, A.B. Yu, G.Q. Lu, Synthesis of polymer montmorillonite nanocomposites by in situ intercalative polymerization, Nanotechnology, 13 (2002) 549–553.
[47] C. Li, Y. Wei, A. Liivat, Y. Zhu, J. Zhu, Microwave-solvothermal synthesis of Fe_3O_4 magnetic nanoparticles, Mater. Lett., 107 (2013) 23–26.
[48] J. Li, H. Yuan, G. Li, Y. Liu, J. Leng, Cation distribution dependence of magnetic properties of solgel prepared $MnFe_2O_4$ spinel ferrite nanoparticles, J. Magn. Magn. Mater., 322 (2010) 3396–3400.
[49] R.M. Khafagy, Synthesis, characterization, magnetic and electrical properties of the novel conductive and magnetic polyaniline/$MgFe_2O_4$ nanocomposite having the core-shell structure, J. Alloys Compd., 509 (2011) 9849–9857.
[50] H. Yan, J. Zhang, C. You, Z. Song, B. Yu, Y. Shen, Influences of different synthesis conditions on properties of Fe_3O_4 nanoparticles, Mater. Chem. Phys., 113 (2009) 46–52.
[51] M.H. Beyki, M. Bayat, F. Shemirani, Fabrication of core–shell structured magnetic nanocellulose base polymeric ionic liquid for effective biosorption of Congo red dye, Biores. Technol., 218 (2016) 326–334.

[52] M. Bayat, M.H. Beyki, F. Shemirani, One-step and biogenic synthesis of magnetic Fe_3O_4-Fir sawdust composite: application for selective preconcentration and determination of gold ions, J. Ind. Eng. Chem., 21 (2015) 912–919.
[53] A. Dabrowski, Adsorption, from theory to practice, Adv. Colloid Interface Sci., 93 (2001) 135–224.
[54] M. Iqbal, N. Iqbal, I. Ahmad, N. Ahmad, M. Zahid, Response surface methodology application in optimization of cadmium adsorption by shoe waste: a good option of waste mitigation by waste, Ecol. Eng., 88 (2016) 265–275.
[55] M. Hossein Beyki, M.H. Ghasemi, A. Jamali, F. Shemirani, A novel polylysine–resorcinol base γ-alumina nanotube hybrid material for effective adsorption/preconcentration of cadmium from various matrices, J. Ind. Eng. Chem., 46 (2017) 165–174.
[56] R. Khani, S. Sobhani, M.H. Beyki, Highly selective and efficient removal of lead with magnetic nano-adsorbent: multivariate optimization, isotherm and thermodynamic studies, J. Colloid Interface Sci., 466 (2016) 198–205.
[57] B. Pan, B. Xing, Adsorption mechanisms of organic chemicals on carbon nanotubes, Environ. Sci. Technol., 42 (2008) 9005–9013.
[58] M. Bayat, F. Shemirani, M.H. Beyki, Utilization of facile synthesized Fe_3O_4 nanoparticles as a selective support for preconcentration of lead ions from food and environmental samples, Anal. Methods, 6 (2014) 5345.
[59] W. Song, B. Gao, X. Xu, L. Xing, S. Han, P. Duan, W. Song, R. Jia, Adsorption-desorption behavior of magnetic amine/Fe_3O_4 functionalized biopolymer resin towards anionic dyes from wastewater, Biores. Technol., 210 (2016) 123–130.
[60] J. Li, Q. Fan, Y. Wu, X. Wang, C. Chen, Z. Tang, X. Wang, Magnetic polydopamine decorated with Mg-Al LDH nanoflakes as a novel bio-based adsorbent for simultaneous removal of potentially toxic metals and anionic dyes, J. Mater. Chem. A, 4 (2016) 1737–1746.
[61] A. Sari, D. Mendil, M. Tuzen, M. Soylak, Biosorption of Cd(II) and Cr(III) from aqueous solution by moss (*Hylocomium splendens*) biomass: equilibrium, kinetic and thermodynamic studies, Chem. Eng. J., 144 (2008) 1–9.
[62] T. Maneerung, J. Liew, Y. Dai, S. Kawi, C. Chong, C.H. Wang, Activated carbon derived from carbon residue from biomass gasification and its application for dye adsorption: kinetics, isotherms and thermodynamic studies, Biores. Technol., 200 (2016) 350–359.
[63] L. Sun, D. Chen, S. Wan, Z. Yu, Performance, kinetics, and equilibrium of methylene blue adsorption on biochar derived from eucalyptus saw dust modified with citric, tartaric, and acetic acids, Biores. Technol., 198 (2015) 300–308.
[64] N.K. Goel, V. Kumar, N. Misra, L. Varshney, Cellulose based cationic adsorbent fabricated via radiation grafting process for treatment of dyes waste water, Carbohydr. Polym., 132 (2015) 444–451.
[65] S. Lin, Heavy metal removal from water by sorption using surfactant-modified montmorillonite, J. Hazard. Mater., 92 (2002) 315–326.
[66] M.M. Saeed, Adsorption profile and thermodynamic parameters of the preconcentration of Eu(III)-on 2-thenoyltrifluoroacetone loaded polyurethane (PUR) foam, J. Radioanal. Nucl. Chem., 256 (2003) 73–80.
[67] A. Dada, A. Olalekan, A. Olatunya, O. Dada, Langmuir, Freundlich, Temkin and Dubinin–Radushkevich isotherms studies of equilibrium sorption of Zn^{2+} unto phosphoric acid modified rice husk, IOSR J. Appl. Chem., 3 (2012) 38–45.
[68] O. Redlich, D.L. Peterson, A useful adsorption isotherm, J. Phys. Chem., 63 (1959) 1024–1024.
[69] K.Y. Foo, B.H. Hameed, Insights into the modeling of adsorption isotherm systems, Chem. Eng. J., 156 (2010) 2–10.
[70] P. Senthil Kumar, S. Ramalingam, C. Senthamarai, M. Niranjanaa, P. Vijayalakshmi, S. Sivanesan, Adsorption of dye from aqueous solution by cashew nut shell: studies on equilibrium isotherm, kinetics and thermodynamics of interactions, Desalination, 261 (2010) 52–60.
[71] H. Shahbeig, N. Bagheri, S.A. Ghorbanian, A. Hallajisani, S. Poorkarimi, A new adsorption isotherm model of aqueous solutions on granular activated carbon, World J. Model. Simul., 9 (2013) 243–254.
[72] Z.S. Kardar, M.H. Beyki, F. Shemirani, Development of an efficient enrichment system for copper determination in water and food samples based on p-phenylenediamine anchored magnetic titanium dioxide nanowires, Int. J. Environ. Anal. Chem., 96 (2016) 1276–1289.
[73] M.J. Aghagoli, M.H. Beyki, F. Shemirani, Application of dahlia-like molybdenum disulfide nanosheets for solid phase extraction of Co (II) in vegetable and water samples, Food Chem., 223 (2017) 8–15.